Stochastic simulation of woven composites forming

A.A. Skordos, M.P.F. Sutcliffe

Accepted Manuscript

Stochastic simulation of woven composites forming

A.A. Skordos, M.P.F. Sutcliffe

PII: S0266-3538(07)00067-X
DOI: 10.1016/j.compscitech.2007.01.035
Reference: CSTE 3600

To appear in: *Composites Science and Technology*

Received Date: 3 November 2006
Revised Date: 16 January 2007
Accepted Date: 26 January 2007

Please cite this article as: Skordos, A.A., Sutcliffe, M.P.F., Stochastic simulation of woven composites forming, *Composites Science and Technology* (2007), doi: 10.1016/j.compscitech.2007.01.035

Stochastic simulation of woven composites forming

A. A. Skordos* and M. P. F. Sutcliffe

Department of Engineering, University of Cambridge, Trumpington Street, Cambridge, CB2 1PZ, UK

Abstract

A stochastic forming simulation procedure is developed and implemented to investigate the effect of geometric variability in pre-impregnated woven textiles on manufacturing. Image analysis is used to characterise variability in tow directions and unit cell size in a pre-impregnated carbon/epoxy satin weave textile. It is found that variability in tow orientations is significant, whereas variability in the unit cell size is negligible. Variability in the weft direction is higher than in the warp direction. Highly anisotropic spatial autocorrelation of weft tow orientations is observed with the major direction of autocorrelation normal to the corresponding set of tows. The extent of autocorrelation is 6 to 20 unit cells. The autocorrelation structure is modelled using a two-parameter stochastic process, the Ornstein-Uhlenbeck sheet, and an efficient parameter estimation technique is developed based on maximum likelihood. The resulting stochastic process is simulated using Cholesky decomposition which is combined with a simplified forming model within a Monte Carlo scheme. The forming model incorporates non-linear strain-rate dependent behaviour and wrinkling due to tow buckling in a truss formulation. Execution of the integrated scheme shows that geometric variability of the woven material has significant influence on the forming process. The coefficient of variation of minimum and average wrinkling strain in the formed component is in the range of 10% to 20%. Variability affects the results of forming optimisation and it should be taken into account in process design. Although applied to the case of woven textile forming, the stochastic scheme presented in this paper is general and can be applied to any material system with imperfect structure.

Keywords: A. Fabrics/textiles; A. Textile composites; C. Statistics; E. Forming

* Corresponding author
E-mail address: aas46@cam.ac.uk
Telephone: +44 1223 333443
Fax: +44 1223 332662

1. Introduction

Fabrication of continuous fibre reinforced thermosetting matrix composites involves processes of different physical nature, including forming, consolidation or impregnation, and curing. Each of the processes influences subsequent manufacturing stages, and feeds through to the design of the composite component, creating complex interdependencies between manufacturing parameters, design constraints and properties of the final part. Process models simulating the different stages of manufacturing have been developed during the last decades and applied to the majority of processing techniques [1-6]. These models, which assume that properties and geometrical features are deterministic, have played an important role in understanding process outcome sensitivity and in developing process design and optimisation schemes. A gap exists between deterministic process simulation and industrial practice, as practical fabrication of composite components is performed in an environment of significant uncertainty both in material properties and in process parameters. The main sources of uncertainty in composite processing are (i) variations in fibre architecture which can be introduced during manufacturing, storage and handling of dry fabrics and pre-impregnated textiles; (ii) variations in the matrix material which can be caused by batch to batch variations in resin formulation and composition, or by variability in storage conditions; and (iii) variations in process conditions related to environmental parameters and control tolerances.

Variations in fibre architecture of textiles may affect the outcome of the draping/forming stage and introduce uncertainty in permeability and in thermal properties that play a significant role in subsequent processes such as filling/consolidation and cure. Furthermore, variability in the textile material causes local disturbances in the fibre architecture which in turn affect the local elastic properties and strength The extent and spatial distribution of these variations determines their significance with respect to the expected properties used in component design. For example, in the case of unidirectional composites it has been demonstrated that the spatial character of fibre misalignment has a significant effect on compressive strength [7]. Variations in the matrix material affect the curing stage with potential consequences in the final material state. Uncertainty in process parameters includes variations in thermal and pressure boundary conditions as well as in tooling properties, and can potentially affect all stages of manufacturing and the quality of produced components. These effects should be taken into account in

process design with the incorporation of variability in appropriate stochastic process simulations to enable evaluation of potential process designs in terms of process robustness to be made.

The issue of variability and its influence on composites manufacturing has received relatively little attention. The combination of draping simulations with fibre misalignment information for non-crimp fabrics within a simplified Monte Carlo scheme has demonstrated the significance of variability in forming [8]. This used a simplified model of fibre misalignment which did not consider spatial correlations. It is expected that variations in fibre architecture of textiles are not distributed uniformly over a region of material, as fibre continuity and friction at tow crossovers (in the case of woven textiles) force disturbances to spread to neighbouring locations. Consequently, a realistic model for variability in forming with these materials requires information on the spatial structure of material variables, in addition to their global variance. The effect of process and material uncertainty on the variability of fill time in liquid composite moulding has been shown to be significant [9]. Fabric permeability variations can be attributed to both fibre angle and fibre spacing variability [10-14]. Stochastic simulation of the filling stage in liquid moulding has been performed using both normally distributed spatially uncorrelated geometrical variability [10] and a random field in which spatial structure is taken into account [11, 14]. It was concluded that quantitative prediction of variability requires consideration of the spatial structure. Computational and experimental efforts have also demonstrated that dry spot formation in liquid moulding is controlled by stochastic effects caused by fabric heterogeneity due to variable nesting of adjacent layers [15, 16]. Padmanabhan and Pitchumani [17] examined the influence of variability on curing of composites. Parameters of cure kinetics models and cure temperature were assumed to be random with coefficient of variation in the range of 1.5%-5%, and it was found that uncertainty induces significant variations in cure completion times. Furthermore, incorporation of uncertainty affects the results of cure optimisation [18, 19]. The effect of the variability of relevant material properties on the dimensions of produced components has also been found to be significant [20]. The results reported in these studies indicate the general importance of variability in fabrication of composites and highlight the need for development of appropriate stochastic modelling methodologies and tools for composite manufacturing processes. The focus is on the adaptation of stochastic simulation techniques which have found wide application in other branches of applied science and engineering such as geophysics, spatial

economics, image and signal analysis, as well as on the development of variability characterisation techniques for the generation of the necessary experimental information.

This study aims at the investigation of the influence of fibre architecture parameters on the forming of woven composites. An image analysis methodology is developed to measure local fibre architecture parameters, such as fibre tow directions and the dimensions of the woven textile unit cell. This is used to derive the distribution in these properties for a pre-impregnated carbon epoxy woven textile. A stochastic model describing the autocorrelation structure based on the Ornstein-Uhlenbeck sheet is used and maximum likelihood estimation yields the model parameters in the example of the carbon epoxy pre-impregnated textile. This statistical description of the textile is used to generate numerical realisations of the woven material for use in a forming analysis. The results of a Monte Carlo simulation for uniform and variable blank holder force distributions are compared to evaluate the influence of taking into account material variability in process design.

2. Analysis of geometric variability of woven materials

Investigation of variability in the geometrical parameters of woven materials requires development and application of an image analysis procedure which operated at a local level. Here, the focus is to estimate tow directions and unit cell lengths in the tow directions by assuming approximate a priori knowledge of the size of the unit cell of the textile.

2.1. Image analysis methodology

A grey-scale image of the woven textile can be represented by a function $f(x,y)$ expressing the distribution of brightness with $F(u,v)$ its Fourier spectrum. The structure of woven textiles is periodic and can be described as a convolution of an elementary unit $u(x,y)$ by a pattern of repetition $h(x,y)$ [21]

$$f(x,y) = u(x,y) \otimes h(x,y) \tag{1}$$

with the pattern of repetition expressed as

$$h(x,y) = \sum_{n,m \in Z} d\left(x - na_x - mb_x, y - na_y - mb_y\right) \tag{2}$$

where $d(x,y)$ is the Dirac delta function and $\{\mathbf{a} = (a_x, a_y), \mathbf{b} = (b_x, b_y)\}$ is the vector basis that generates $h(x,y)$. It should be noted that the decomposition implied by Eq. (1) is not unique and several elementary

unit-vector basis combinations can generate the same periodic structure. The image analysis technique estimates the local basis vector $\{\mathbf{a},\mathbf{b}\}$ that corresponds to a conventional rectangular unit cell.

Fourier transform of a linear periodic image yields a two dimensional spectrum with directional structure with maxima in the direction normal to the orientation of the image. This fact has been used in image analysis of woven textiles to estimate the direction of tows by integrating $|F(u,v)|$ along radial directions and identifying the warp and weft direction as the directions of maximum accumulated radial energies [22]. Furthermore, the number of tows per unit length is related to the distance between the dc term, i.e. the point of zero frequency, and the first peak of $|F(u,v)|$ in the corresponding tow direction [21]. Based on these principles and the use of the fast Fourier transform (FFT) computationally efficient methodologies for analysing woven textile images have been developed and applied to automated defect detection and weave pattern identification in textiles [23, 24]. The applicability of these techniques in the context of the present study is limited as they are based on the analysis of images comprising a large number of unit cells of the periodic structure. Here, estimation of local geometric variables at a unit cell level is required and Fourier transform is only useful for a pre-estimation of tow directions. This information is combined with the nominal unit cell size to obtain a prior estimate of unit cell positions adjacent to the centre of the image of the woven material. Correlation analysis is then employed for an accurate estimation of the position of adjacent cells. The correlation of a reference region $r(x,y)$ with the image $f(x,y)$ at location (t_x,t_y) is

$$C(t_x,t_y)=\iint_O r(x,y)f(x+t_x,y+t_y)dxdy \tag{3}$$

with the reference region O selected to coincide with the central part of the image. Correlation reaches a maximum value at the centre of the image and, due to periodicity, high peak values at points of repetition adjacent to the centre. Thus, it is possible to identify the local basis vector of the pattern of repetition in terms of tow directions and unit cell size in the tow directions.

The image analysis procedure is performed in seven steps as follows:

(i) Image acquisition and digitisation into a $K\times K$ discrete pixel array $f(x,y)$.

(ii) Application of fast Fourier transform to calculate $F(u,v)$ and the modulus $|F(u,v)|$.

(iii) Calculation of radial energy $E(?)$ after expressing F in polar coordinates as $E(?)=\int_0^{+\infty}|F(r,?)|dr$.

(iv) Estimation of approximate directions $\hat{?}_1$ and $\hat{?}_2$ that maximise $E(?)$.

(v) Estimation of an initial solution for the basis vector $\{\hat{\mathbf{a}},\hat{\mathbf{b}}\}$ using the approximate tow directions and the nominal unit cell size. A prior estimate of the position of the four unit cells adjacent to the centre of the image is then found from the approximate basis vector.

(vi) Calculation of correlation in the vicinity of the prior estimates of unit cell position using a central reference region $r(x,y)$ of size $M\times M$ by the expression

$$?(t_x,t_y)=\frac{\sum_{i=1,j=1}^{M,M}\left(r(x_i,y_j)-\bar{r}\right)\left(f(x_i+t_x,y_{j_y})-\bar{f}\right)}{\sqrt{\sum_{i=1,j=1}^{M,M}\left(r(x_i,y_j)-\bar{r}\right)^2\sum_{i=1,j=1}^{M,M}\left(f(x_i+t_x,y_{j_y})-\bar{f}\right)^2}} \quad (4)$$

where $\bar{r}$ and $\bar{f}$ denote the average of the $M\times M$ and $K\times K$ arrays. Correlation is normalised in Eq. (4) so that a value of 1 is obtained at the centre of the image. This calculation is computationally intensive and therefore it is performed over a region with a size approximately equal to 20 % of the nominal unit cell size, centred at each prior estimate of the unit cell positions.

(vii) Estimation of the positions that maximise $?(t_x,t_y)$ and calculation of the basis vector and the tow directions and unit cell size.

The image analysis methodology was applied to images of a five harness satin weave 6k carbon/epoxy pre-preg (Hexcel) with a resin weight fraction of 0.42. The fibre areal weight of this pre-preg is 370 g/m^2, its linear tow density is 4.5 tows/cm and the width of tows 2.2 mm. Digital images were acquired using an Olympus camera. The woven material was set on the table of an Omicron coordinate measurement system, while the camera was mounted on its measuring head in order to record the exact position of each image. Four hundred and sixty images were acquired on a 23 × 20 grid with 15 mm spacing. Fig. 1 shows an image of the textile, with the corresponding FFT spectra and correlation distributions. The results of image analysis, illustrated as four lines starting from the centre of each image and ending at the estimated location of the adjacent unit cells, are superimposed on the woven material image. The nominal unit cell is 10 mm, the size of the image array is 480 × 480 and the size of the reference region is 70 × 70. It should be noted that the FFT spectra in Fig. 1(b) are rotated by 90^o to

illustrate the coincidence of maximum radial energy directions with the direction of tows. The spectra obtained by the Fourier transform are sharp and correlation estimates exhibit very sharp peaks. This allows accurate estimation of unit cell positions.

2.2. Statistical properties and spatial autocorrelation

The basic statistical properties of the unit cell parameters of the carbon/epoxy textile are summarised in Table 1, and the correlation matrix is given in Table 2. The corresponding distributions are illustrated in Fig. 2. Here, $?_{warp}$, $?_{weft}$ denote the warp and weft directions respectively. Angles are measured in a clockwise direction relative to the nominal warp direction of the material. The unit cell lengths in the two tow directions are l_{warp} and l_{weft}, while l_o is the nominal unit cell length. Unit cell lengths are expressed as percentage ratios with respect to nominal lengths. The statistical properties reported include the average μ and the standard deviation s of the sample. Also, the single measurement standard deviation, s_r, calculated from the analysis of 20 images taken at the same location of the woven sheet, and the standard deviation due to uncertainty, s_u, calculated as the error due to the finite resolution of the images are reported. It can be observed that there exists significant variability in both tow directions. Variability in warp tow orientations appears significantly lower than that for the weft direction. Variability in unit cell lengths is negligible, since the sample standard deviation is of similar magnitude to repeatability for this material. The correlation matrix (Table 2) indicates that the two tow directions are uncorrelated which implies that variability in warp and weft tows is generated independently. Also, the two unit cell lengths are uncorrelated and tow directions are uncorrelated to lengths. Examination of the distribution of tow directions and cell lengths shown in Fig. 3 suggests that all variables are normally distributed. The value of warp direction ranges from -1^o to 1^o and of weft direction from 87^o to 92^o. The range of values for the normalised cell length is about 5% in the warp and weft directions with these deviations being of similar magnitude to the repeatability of the image acquisition and analysis procedure.

The autocorrelation structure of the variables of interest is examined in order to quantify the spatial dependence of variability. Spatial autocorrelation is estimated as a function of distance and orientation using the method of moments. The correlation between two samples of all pairs of points in the original sample that are located at a specific distance and orientation, and within a discretisation

range, is calculated. The directional spatial autocorrelation of the stochastic variables for the carbon/epoxy satin weave pre-preg is illustrated in Fig. 3. It can be observed that strong autocorrelation exists in the orientation of weft tows, whereas the autocorrelation in warp tow orientations is negligible. The autocorrelation of weft orientation is persistently high in the 0^o direction, which coincides with the direction of warp tows. Autocorrelation in this direction persists within the range of measurements indicating the existence of variability trends with range that exceeds that of the measurements. These differences between warp and weft tows reflect the differences in tow tensions during the weaving process. Autocorrelation in directions close to the weft direction ($\pm 75^o$) crosses the zero level at about 60 mm, a distance that corresponds to 6 unit cells. Autocorrelation drops off within 10 to 20 unit cells (100 - 200 mm) at orientations between the warp and the weft direction. Negative weft orientation autocorrelation is observed at high distance for directions of fast decaying autocorrelation as a result of longer range trends in the stochastic variable. Curves corresponding to opposite directions in Fig. 3(b) are very similar (compare the dashed and solid lines in Fig. 3). Consequently, the spatial structure of weft tow misalignment in the carbon/epoxy woven pre-preg used in this study is quadrant symmetric. Autocorrelation results for the unit cell lengths in the two directions are not presented here as lengths do not show significant variability. Spatial cross correlation between the warp and weft direction and between lengths and tow orientations is also found to be negligible.

3. Stochastic textile simulation

3.1. Modelling of the random field

The results of spatial analysis showed that misalignment in weft tows of the woven material has an anisotropic spatial autocorrelation structure. The random field, $Z(x,y)$, generated by this structure and expressing the distribution of the stochastic variable is modelled using a two-parameter stochastic process, the Ornstein-Uhlenbeck sheet, which is defined as a stationary Gaussian process on the plane with covariance function [25, 26]:

$$E[(Z(x_1,y_1)-E[Z])(Z(x_2,y_2)-E[Z])] = s^2 e^{-?_1|x_1-x_2|-?_2|y_1-y_2|} \quad (5)$$

Here $E[\cdot]$ denotes expectation, s is the standard deviation of the stationary field, and $?_1$, $?_2$ are positive coefficients that control the range and degree of anisotropy of the autocorrelation structure. The Ornstein-

Uhlenbeck sheet expressed by Eq. (5) is the two-dimensional ext ension of the mean reverting stochastic process and the continuous equivalent of autoregressive processes [27].

Estimation of the parameters of the Ornstein-Uhlenbeck sheet is based on the maximisation of the likelihood function. The vector of values of the random variable over the plane $\mathbf{Z}$ follows a multidimensional normal distribution with probability density function

$$p(\mathbf{Z}) = \frac{1}{\sqrt{2^N p^N |\mathbf{S}|}} e^{-\frac{1}{2}(\mathbf{?}-\boldsymbol{\mu})^T \mathbf{S}^{-1}(\mathbf{Z}-\boldsymbol{\mu})} \quad (6)$$

where N the size of the vector, $\mathbf{S}$ the covariance matrix calculated using Eq. (5) and $\boldsymbol{\mu}$ the vector of expected values. Given the vector $\mathbf{Z}_{exp}$ of measured values of the random variable on a regular grid of size $m \times n$ the loglikelihood function is

$$l_{m,n}(s, ?_1, ?_2) = log(p(\mathbf{Z}_{exp})) \quad (7)$$

Loglikelihood is used instead of likelihood to avoid numerical problems, as for long vector s $\mathbf{Z}$ the value of the probability density functions involves very high negative powers. The maximum likelihood estimator of the three parameters of the covariance function based on a realisation over a regular grid of sufficiently large size is strongly consistent, i.e. it converges almost surely to the true parameter values. For limited sizesampling grids, maximum likelihood yields a consistent estimator of the product $?_1 ?_2 s^2$ [28]. Moreover, with x fixed, $Z(x_o, y)$ is a one-dimensional process having $s^2 exp(-?_2 |y_1 - y_2|)$ as the covariance function while, with y fixed, $Z(x, y_o)$ is an one-dimensional process having $s^2 exp(-?_1 |x_1 - x_2|)$ as the covariance function. Ying [29] shows that the maximum likelihood estimators of $?_2 s^2$ and $?_1 s^2$ using $Z(x_o, y)$ and $Z(x, y_o)$ are consistent. Combining these three consistent estimators, parameters $?_1$, $?_2$ and s can be estimated.

Evaluation of the likelihood functions expressed by Eqs. (6) and (7) can be computationally expensive within a maximisation routine when the size of vector $\mathbf{Z}$ is relatively high. Here, maximisation of likelihood is based on the expressions developed by Ying [28, 29] for efficient evaluation of the loglikelihood functions for both the stationary Ornstein-Uhlenbeck process and sheet on regular grids. In the one dimensional case the set of observations is $\{Z(t_i) : i = 1, ..., N\}$, and the loglikelihood function is

$$l_N\left(?,s^2\right)=-\frac{Z^2(t_1)}{2s^2}-\frac{log\left(s^2\right)}{2}-\frac{N\,log(2p)}{2}$$
$$-\frac{1}{2}\sum_{i=2}^{N}log\left[s^2\left(1-e^{-2?(t_i-t_{i-1})}\right)\right]-\frac{1}{2}\sum_{i=2}^{N}\frac{\left[Z(t_i)-Z(t_{i-1})e^{-?(t_i-t_{i-1})}\right]^2}{s^2\left(1-e^{-2?(t_i-t_{i-1})}\right)} \quad (8)$$

In the two dimensional case the ordered sample is $\left\{Z\left(x_i,y_j\right):i=1,...,m;\ j=1,...,n\right\}$, and the loglikelihood function of the Ornstein-Uhlenbeck sheet becomes

$$l_{m,n}\left(?_1,?_2,s^2\right)=-\frac{log\left(s^2\right)}{2}-\frac{mn\,log(2p)}{2}-\frac{1}{2}\sum_{i=2}^{m}log\left[s^2\left(1-e^{-2?_1(x_i-x_{i-1})}\right)\right]$$
$$-\frac{1}{2}\sum_{j=2}^{n}log\left[s^2\left(1-e^{-2?_2(y_j-y_{j-1})}\right)\right]$$
$$-\frac{1}{2}\sum_{i=2}^{m}\sum_{j=2}^{n}log\left[s^2\left(1-e^{-2?_1(x_i-x_{i-1})}\right)\left(1-e^{-2?_2(y_j-y_{j-1})}\right)\right]$$
$$-\frac{1}{2}\frac{z_1^TB^{-1}z_1}{s^2}-\frac{1}{2}\sum_{i=2}^{m}\frac{\left(z_i-e^{-?_1(x_i-x_{i-1})}z_{i-1}\right)^TB^{-1}\left(z_i-e^{-?_1(x_i-x_{i-1})}z_{i-1}\right)}{s^2\left(1-e^{-2?_1(x_i-x_{i-1})}\right)} \quad (9)$$

with $z_i=\left[Z(x_i,y_1),....,Z(x_i,y_n)\right]^T$ and B an $n\times n$ matrix with $B_{ij}=exp\left(-?_2\left|y_i-y_j\right|\right)$.

The weft orientation measurements on a 23×20 grid with 15 mm spacing were used for the estimation of $?_1?_2s^2$ by maximising $l_{23,20}\left(?_1,?_2,s^2\right)$. Maximisation of $l_{23}\left(?_2,s^2\right)$ for the sample of weft orientation on the line $x=0$ provides an estimator for $?_2s^2$ and maximisation of $l_{20}\left(?_1,s^2\right)$ for the sample on the line $y=0$ yields an estimator for $?_1s^2$. Maximisation of the loglikelihood functions expressed by Eqs. (8) and (9) was performed using the Generalised Reduced Gradient Nonlinear Optimisation method implemented in Microsoft Excel [30] and yielded a value of 1.08 for s, 5.97 10^{-3} for g_1 and 2.96 10^{-2} for g_2. The estimation procedure used here extrapolates the results of image analysis over a large size textile sheet. The coefficient values imply that autocorrelation of weft tows orientation extends to about 500 mm in the warp direction (direction parallel to coordinate x) and to about 100 mm in the weft direction (direction parallel to coordinate y). These values correspond to three times the correlation length which amounts to a decay of exponential autocorrelation at about 5%.

3.2. Stochastic simulation

The geometry of a sheet of woven textile can be characterised by the distribution of warp and weft direction and of the unit cell size in the two directions over the plane. In a discretised formulation, the woven sheet is characterised by a vector $\mathbf{V}$ of size $4N$. Vector $\mathbf{V}$ comprises the warp and weft

direction and the size of the unit cell at N different locations and it is assumed to follow a multidimensional normal distribution expressed by the following probability density function

$$p(\mathbf{V}) = \frac{1}{\sqrt{2^{4N} p^{4N} |\mathbf{S_V}|}} e^{-\frac{1}{2}(\mathbf{V}-\boldsymbol{\mu}_\mathbf{V})^T \mathbf{S}_\mathbf{V}^{-1}(\mathbf{V}-\boldsymbol{\mu}_\mathbf{V})} \tag{10}$$

The covariance matrix $\mathbf{S_V}$ and the vector of expected values $\boldsymbol{\mu}_\mathbf{V}$ encompass all the information about the statistics of the four variables, and their spatial autocorrelation and cross-correlation. The multidimensional stochastic process is homogeneous (second order stationary) and expected values and variances for the four variables are constant over the plane.

Generation of realisations of a woven sheet following the statistical properties implied by Eq. (10) is performed using Cholesky factorisation. The covariance matrix $\mathbf{S_V}$ is symmetric and positive definite and it has a Cholesky root $\mathbf{L}$ such that:

$$\mathbf{S_V} = \mathbf{L}\mathbf{L}^T \tag{11}$$

where $\mathbf{L}$ is a triangular matrix. The product of a vector $\mathbf{W}$ of normally distributed independent random variables with the Cholesky root is a vector that follows the statistics required by Eq. (10) so that vector $\mathbf{V}$ can be simulated as follows:

$$\mathbf{V} = \mathbf{L}\mathbf{W} \tag{12}$$

The procedure expressed by Eqs. (11) and (12) is implemented in two steps. The first step, in which the Cholesky root is computed, is computationally intensive but only needs to be executed once. This is followed by a generation step in which realisations of random vector $\mathbf{W}$ are generated and transformed to realisations of vector $\mathbf{V}$ via Eq. (12). The second step has low computational cost and is executed a number of times equal to the number of required textile realisations.

Realisations of $\mathbf{V}$ are translated into realisations of a stochastic textile using the procedure depicted in Fig. 4. Two types of nodes are used to define the grid: (i) regular nodes, shown as closed circles in Fig. 4; and (ii) auxiliary nodes, which are placed at intermediate positions of the grid, shown as open circles in Fig. 4. Auxiliary nodes are located at four positions around a regular node so that the linear segment connecting two auxiliary nodes has the slope and length corresponding to the tow direction and unit cell size of the respective regular node in the appropriate direction. The procedure is executed in three steps, with the first two used for the generation of boundary nodes as illustrated in Figs. 4(a) and

4(b), and the third for generation of internal nodes as shown in Fig. 4(c). The generation of nodes of the vertical boundary requires use of the weft direction and unit cell size in the weft direction. Knowledge of the position of node (1, j-1) in Fig. 4(a) allows calculation of the position of node (1, j), as the midpoint of the linear segment that starts at the higher auxiliary node corresponding to (1, j-1), with slope and length corresponding to the direction and unit cell size of weft tows at position (1, j). Subsequently, the positions of the rest of the auxiliary nodes of node (1, j) are computed using the orientation and unit cell size values in both tow directions. Generation of the horizontal boundary (Fig. 4(b)) follows a similar procedure. The position of node (i-1, 1) is used to compute the coordinates of node (i, 1) and of the corresponding auxiliary nodes. The generation of internal nodes starts from the corner of known boundaries and progresses first horizontally and then vertically so that the positions of nodes (i-1, j) and (i, j-1) are known when the position of node (i, j) is computed. The coordinates of the auxiliary node located between nodes (i-1, j) and (i, j) are calculated using the warp direction data for node (i-1, j). Similarly the calculation of coordinates of the auxiliary node located between nodes (i, j-1) and (i, j) is based on the weft direction data for node (i, j-1). These two auxiliary nodes are the starting points of two linear segments with slope corresponding to the orientation of warp and weft tows at position (i, j) and length corresponding to the size of the unit cell in the warp and weft direction. The intersection between these two linear segments coincides with the position of node (i, j) whereas their ends define the positions of the rest of the auxiliary nodes corresponding to node (i, j). This procedure is repeated to generate a sheet of material with the required size.

In the case of the five harness satin weave carbon/epoxy pre-preg used in this study, the warp and weft orientations are considered to be variable, with the spatial autocorrelation given by Eq. (5); while the unit cell size in both directions does not vary. Fig. 5 illustrates two realisations of the carbon/epoxy pre-preg generated on a 20 × 20 grid with 10 mm spacing and the autocorrelation of simulated weft orientation in the warp direction calculated using the method of moments. It can be observed that the autocorrelation of simulated data is very similar to that measured experimentally. In general, the simulation produces quadrant symmetric autocorrelation structures that reproduce the experimental results illustrated in Fig. 3. Autocorrelation is persistently high in the warp direction, and negative values occur at other directions due to the long range trends induced by the Ornstein-Uhlenbeck

sheet with long correlation lengths. As a result the Ornstein-Uhlenbeck sheet can reproduce the existence of trends over a limited area of the textile which cause negative autocorrelations.

4. Simulation of forming

4.1. Forming model

Forming is modelled using a simplified finite element model based on a truss representation of the woven material. A brief description of the forming model is given here; a full description of its operation, material submodels, convergence and validation can be found in [31]. The simplified forming model simulates the woven fabric as an assembly of bars, as shown in Fig. 6. All bars are connected at the corners of the unit cell via pin joints. The sides of the unit cell represent the tows of the textile and the diagonal bars govern the non-linear shear behaviour of the assembly. This arrangement allows the trellising action observed in practice to be reproduced when the effective stiffness of the tow bars is significantly higher than the shear resistance of diagonal bars. Under shear, one of the diagonal elements is in tension and the other in compression. The incorporation of wrinkling due to tow buckling is based on an activation/deactivation strategy applied to tow elements. Deactivation is triggered by the existence of compressive strain in the element and reactivation by the existence of tensile strain. The action of the blank holder on the woven material is incorporated in a simplified way in the model by the inclusion of a group of bar elements connected to nodes in contact with the blank holder. These elements, which are fixed with respect to all degrees of freedom on their free ends, simulate friction via their perfectly plastic behaviour. Their yield stress is selected to match the total clamping force and the tool-woven sheet friction coefficient.

The material behaviour of tow and diagonal shear elements follows directly from experimental observations and the operational requirements of the simplified model. Tow elements govern the tensile behaviour of the material in the tow direction, which typically follows a bilinear stress-strain curve, with the initial part corresponding to changes in undulation and tow compression and the second part following the elastic behaviour of the tow [32]. A non-linear elastic constitutive relationship is used to express this behaviour,

$$s_t = E_8 e_t + \frac{E_o - E_8}{a} ln\left(\frac{1}{1+e^{-a(e_t-\bar{e})}}\right) - \frac{E_o - E_8}{a} ln\left(\frac{1}{1+e^{a\bar{e}}}\right) \quad (13)$$

Here s_t and e_t denote the tow element stress and Green-Lagrange strain respectively, E_o is the effective tow modulus at very low strains, E_8 the effective modulus at high strains. The transition from the low modulus region to the high modulus region occurs at a transition strain $\bar{e}$ and has breadth proportional to $1/a$. This simplified non-linear elastic model adopted here, neglects the coupling between warp and weft tow tensile strains seen in textiles modelling, though in principle this could be incorporated. The incorporation of wrinkling due to tow buckling is implemented by deactivating tow elements that are under compression, which is equivalent to setting the tow stress equal to zero.

Shear diagonal elements follow an elastic-viscoplastic phenomenological constitutive model that reproduces the non-linear behaviour of woven textiles and incorporates strain rate dependence. Typically, woven materials show high shear compliance at low strains when bearing-type contact effects dominate deformation, while their shear resistance increases rapidly at higher strains due to lateral compression and intra-tow friction which eventually cause lock up of the textile [33]. The strain of shear elements is decomposed into viscoelastic and viscoplastic contributions as

$$e_d = e_d^{vp} + e_d^{ve} \tag{14}$$

The element follows a viscoelastic law when strain is below a yielding strain or when the stress and strain rates have opposite signs,

$$s_d + \dot{s}_d \frac{?}{E_p} = E_p e_d^{ve} + \frac{E_p + E_v}{E_v} ?\dot{e}_d \tag{15}$$

where s_d denotes the element stress, E_p and E_v are the moduli of the elastic-viscoplastic model and $?$ is the viscosity of the model.

When the viscoelastic strain exceeds the yield limit and the sign of stress is the same as that of strain rate the material behaves viscoplastically and

$$s_d + \dot{s}_d \frac{?}{E_v} = \pm s_o + ?\dot{e}_d \tag{16}$$

where the plus sign corresponds to tension and minus to compression. Here s_o denotes the yield stress of the element.

A generalisation of the elastic-viscoplastic constitutive model that includes strain dependent viscosity [34] is used by adopting the following relationship

$$?\left(e_d^v\right)=\begin{cases} ?_o\left[1+s_8\left|e_d^v\right|+\dfrac{s_o-s_8}{a_v}ln\left(\dfrac{1}{1+e^{-a_v\left(\left|e_d^v\right|-\bar{e}_v\right)}}\right)\right. \\ \qquad \left.-\dfrac{s_o-s_8}{a_v}ln\left(\dfrac{1}{1+e^{a_v\bar{e}_v}}\right)\right] & e_d^v\dot{e}>0 \\ ?_o & e_d^v\dot{e}<0 \end{cases} \tag{17}$$

where e_d^v is the viscous strain of the viscous element of the model given as

$$e_d^v=e-\frac{s-E_p e_d^{ve}}{E_v} \tag{18}$$

The dependence of viscosity on the viscous strain follows a bilinear curve when the viscous element is in tension and the strain rate is positive, or when the viscous element is in compression and the strain rate negative (corresponding to loading of the element either in tension or compression). In this region, the slope of the bilinear curve is $?_o s_o$ at low absolute viscous strains and $?_o s_8$ at high absolute viscous strains. Transition from one behaviour to the other occurs at absolute viscous strain $\bar{e}_v$ with a breadth proportional to $1/a_v$. In unloading, i.e. when strain rate and viscous strain have opposite signs, the viscosity has a constant value.

4.2. Material properties

The results of tensile and bias extension test were used to estimate material parameters involved in the material submodels described by Eqs. (13)-(15). Tests were performed on the 5 harness 6k carbon/1947 epoxy satin weave. Tensile experiments were carried out on an Instron test machine at a deformation rate of 2 mm/min. A gauge length of 10 cm was used and the deformation was measured using a laser extensometer. The load was applied using clamps of 2.5 cm width which was equal to the width of the samples. Bias extension tests were carried out using the equipment described in [35]. A rectangular piece of woven material, 210 mm × 70 mm in dimensions, was loaded with the warp and weft directions orientated initially at ± 45^o to the loading. Three test speeds were used, 10, 40 and 160 mm/min corresponding strain rates of 0.0013, 0.0055 and 0.022 s^{-1} respectively. The applied force and the deformation of the diagonal of a square gauge region with an initial diagonal size of 40 mm in the full shear part of the specimen were recorded.

Fig. 7 illustrates the results of tensile and bias extension characterisation experiments. The typical bilinear behaviour caused by decrimping effects is observed in tension. Bias extension results show an initial force increase at low strains, followed by a low stiffness region and a large increase in stiffness at high strains. Strong strain rate dependence of the response in bias extension is observed. Apparent shear compliance decreases with increasing rate, whereas the strain at which a transition from low to high shear stiffness behaviour occurs increases. Measured force is normalised by the number of tows of the corresponding specimen (11 tows in the tensile test and 22 in the bias extension test) to calculate tow stress used in material submodels. Inversion of Eqs. (13) - (18) is performed to estimate material parameters that minimise the discrepancy between model and experimental response. Details of the integration scheme used for Eqs. (13)-(18), of the inversion technique and of the selection of initial values are given in [31]. The results of model fitting are summarised in Table 3. The average error is 1.8 N in tensile force estimation and 1 N in bias extension which corresponds to 0.5 % and 7 % relative error respectively. The quality of the fit is illustrated in Fig. 7. The tensile curve is followed closely by the model. The general form of the bias extension simulation results matches the experiments and strain rate dependence is reproduced successfully.

4.3. Deterministic forming simulation

The forming model accompanied by the material submodels is implemented in MSC.Marc to model the forming of a hemisphere. The radius of the hemisphere considered is 60 mm. A fillet with a radius of 20 mm connects the hemisphere with a tool base. Appropriate user defined subroutines are used to incorporate the viscoplastic stress-strain response of shear elements, wrinkling and the non-linear elastic behaviour of tow elements and the perfectly plastic behaviour of friction elements. Material properties produced by experimental analysis and parameter identification are normalised with respect to the number of tows, and properties of the elements of the unit cell are scaled accordingly. Tooling is modelled as a group of rigid surfaces and contact between the tow elements of the woven sheet and tooling is considered. In the deterministic case, the woven material has an ideal geometry and quadratic symmetry can be used. In stochastic simulation, however, geometry deviates from the ideal case and consideration of the full geometry of the model is necessary.

Investigation of mesh convergence has indicated that a unit cell size of 15 mm is adequate for simulation of draping over a hemisphere with the geometry used here [31]. Optimisation studies have

indicated that use of variable peripheral force involving higher clamping pressures at positions aligned to the bias direction of woven textiles minimises wrinkling due to tow buckling in the produced component [36]. Hemisphere forming using the five harness satin weave carbon/epoxy pre-preg was investigated using the deterministic forming simulation. Two cases are considered: (i) forming with constant peripheral force profile; and (ii) forming with variable force profile. The total clamping force applied to the sheet of woven material is 400 N in both cases. In the variable peripheral pressure case force in the bias direction, i.e. along the diagonal of the woven sheet, is increased by 75%.

Table 4 summarises the results of deterministic forming simulation and Fig. 8 illustrates a comparison of formed patterns, textile shear distribution and wrinkling strain distribution under uniformly distributed and under variable clamping pressure. High shear occurs at four locations aligned to the bias direction near the base of the hemisphere. Shear on the apex and at normal positions near the base is negligible. Maximum shear is slightly higher in the case of the optimised force profile as a consequence of increased force in the direction of high shear. The model identifies regions of concentrated wrinkling due to tow buckling at four normal positions aligned to the tow directions along the base of the hemisphere. The direction of compression due to wrinkling is parallel to the corresponding side of the base at each of the four locations. The maximum absolute value of wrinkling strain decreases from 10 % to 8 % when the variable peripheral force is used, while average absolute wrinkling strain over the hemisphere decreases from 0.24 % to 0.14 %. This follows from the fact that the mechanisms of wrinkling due to tow buckling and shear are competitive modes of deformation as the woven textile conforms on the doubly curved tool. Conditions that promote higher shear, such as increased force in diagonal directions, result in less wrinkling.

4.4. Stochastic forming simulation

The stochastic textile generation procedure described previously is coupled with the forming model to carry out stochastic process simulation. The interaction between textile generation and the process model is performed by altering nodal coordinates in the MSC.Marc finite element input file. The forming model is executed for 400 realisations of the stochastic representation of the five harness carbon/epoxy satin weave pre-preg using the constant and variable force profiles described in the previous section. For this material, the unit cell size is considered to be deterministic according to the results of image analysis. The direction of warp tows is stochastic with standard deviation of 0.36^{o}. Weft

tow direction is stochastic and spatially autocorrelated with a structure that follows the Ornstein-Uhlenbeck sheet described by Eq. (5). Cross-correlations between the various variables are negligible.

Fig. 9 illustrates the distributions of average and minimum wrinkling strain for the two peripheral force profiles produced from these runs, alongside the corresponding values for the case of a textile with ideal geometry. The results indicate that average and minimum wrinkling strain follow a normal distribution. As reported in the previous section, both the average and minimum wrinkling strain for uniform material geometry decreasesignificantly when the variable peripheral force profile is used. Similarly in the stochastic case with variable textile geometry the distributions are shifted to higher strains with the variable peripheral force profile. Average wrinkling with a uniform force is approximately equal to the result of the ideal textile forming simulation. In contrast, average wrinkling with the optimised force profile is lower than that of the deterministic case, indicating an adverse effect of the use of the optimised profile on the robustness of the process. Minimum wrinkling is significantly lower than minimum wrinkling in the ideal material case. Consequently, the ideal material result corresponds to approximately 90% of the stochastic simulation result, i.e. about 90% of the stochastic simulation realisations show more absolute wrinkling than the ideal geometry simulation. These results indicate that the variability of woven textiles induces significant variability in the outcome of the forming process. For the carbon/epoxy pre-preg investigated in this study variability corresponds to a coefficient of variation in the range of 10-20 % for average and minimum wrinkling strain.

Table 5 provides a comparison between the statistics of wrinkling in the two tow directions. It can be observed that the mean and variance of both the average and minimum wrinkling are the same for the warp and weft directions, so that wrinkling results for two directions can be aggregated. The nonlinearity in the calculation of minimum wrinkling results in higher average and similar standard deviation for the aggregate. The correlation between average wrinkling in the warp and weft direction is negative with a value of approximately -0.4 for both the uniform and variable force profile. As a result, the standard deviation of average wrinkling strain over both warp and weft tows is significantly lower than the standard deviation in any of the two directions.

Fig. 10 illustrates the wrinkling strain distribution for the uniform and variable force profile for one realisation of the stochastic forming simulation. It can be observed that the distribution is asymmetric and for this realisation wrinkling strain in the warp direction is higher than in the weft direction.

Wrinkling due to tow buckling occurs at similar positions as those predicted in deterministic forming simulation. However, in the stochastic case, the exact location can be slightly different, e.g. for buckling of warp tows in the case of uniform force profile in the realisation shown in Fig. 10.

5. Conclusion

In this study, a methodology is presented for analysing and simulating random geometrical parameters of woven materials, which are expected to influence forming and final properties of woven composite structures. Image analysis provides quantitative information on misalignment of tows and local unit cell size. The methodology proposed in this study is based on a combination of Fourier transform, which provides an approximate estimate of warp and weft tow directions, and a local correlation search which yields accurate estimates of the position of unit cells adjacent to the centre of an image of the woven material. The analysis is applied to images of a five harness carbon/epoxy satin weave pre-preg. It is observed that variability of tow orientations is significant and tends to be higher in the weft direction than in the warp direction. In contrast, unit cell lengths do not show significant variations. Cross-correlations between all variables are found to be negligible. The orientation of weft tows in the carbon/epoxy pre-preg has a strong and highly anisotropic spatial autocorrelation. Persistent correlation of weft orientation occurs at its corresponding normal direction. Autocorrelation drops off within 6 to 20 unit cell lengths at directions other than the normal.

The random field resulting from spatially autocorrelated stochastic variables is simulated using the Ornstein-Uhlenbeck sheet. Cholesky decomposition is employed to simulate the stochastic variables of the woven textile over the plane. Stochastic simulation generates the values of the warp and weft orientation, and unit cell size in the warp and weft direction on a grid. This information is translated into a realisation of the stochastic woven textile by computing the coordinates of the nodes of the grid.

Stochastic simulation is coupled with a simplified finite element model of forming to quantify the effect of woven material variability on the formed component. The model is based on a truss approximation of the textile and it incorporates non-linear rate dependent shear of the woven material and wrinkling due to tow buckling. Results show that variability of the woven material geometry induces significant variations in the formed component. Coefficient of variations of average and minimum wrinkling strain in the formed component are in the range 10-20 %. In addition, forming conditions which

were found to be optimal in a deterministic optimisation framework are still preferable but introduce higher variability in the final geometry when the stochastic nature of the textile is considered.

The stochastic formulation presented here can be expanded to incorporate variability information arising from sources of uncertainty other than fibre architecture, such as process parameters and resin matrix properties. Future work will use this simulation scheme in conjunction with optimisation tools in order to incorporate information on process sensitivities and performance-variability trade offs in process design.

Acknowledgements

Contributions from the EPSRC, MSC.Software Ltd, University of Nottingham, DSTL, UK Ministry of Defence, Hexcel Composites, Granta Design Ltd., Ford Motor Company Ltd., Polynorm Plastics (UK) Ltd., Virtual Prototyping Solutions Ltd., Saint-Gobain Vetrotex International SA and ESI Software SA are gratefully acknowledged.

References

1. Loos AC, Springer GS. Curing of epoxy matrix composites. J Compos Mater 1983;17(2):135-169.
2. Van Der Weeen F. Algorithms for draping fabrics on doubly curved surfaces. Int J Numer Meth Eng 1991;31(7):1415-1426.
3. Bogetti TA, Gillespie JW. Two-dimensional cure simulation of thick thermosetting composites. J Compos Mater 1991; 25(3): 239-273.
4. Long AC, Blanchard PJ, Rudd CD, Smith P. The development of an integrated process model for liquid composite moulding. Compos Part A-Appl S 1998;29(7):847-854.
5. Pillai KM, Advani SG. A model for unsaturated flow in woven fiber preforms during mold filling. J Compos Mater 1998;32(19): 1753-1783.
6. Dong L, Lekakou C, Bader MG. Solid-mechanics finite element simulations of the draping of fabrics: a sensitivity analysis. Compos Part A-Appl S 2000;31(7):639-652.
7. Liu D, Fleck NA, Sutcliffe MPF. Compressive strength of fibre composites with random fibre waviness. J Mech and Phys Solids 2004;52(7): 1481-1505.

8. Yu WR, Harrison P, Long AC. Finite element forming simulation of NCF considering variability of fiber direction. Proceedings of the 8th ESAFORM Conference on Material Forming, Cluj-Napoca, Romania, 2005. p. 963-966.

9. Padmanabhan SK, Pitchumani R. Stochastic modeling of nonisothermal flow during resin transfer molding. Int J Heat Mass Tran 1999;42(16):3057-3070.

10. Endruweit A, Long AC, Robitaille F, Rudd CD. Influence of stochastic fibre angle variations on the permeability of bi-directional textile fabrics. Compos Part A-Appl S 2006;37(1):122-132.

11. Endruweit A, Long AC. Influence of stochastic variations in the fibre spacing on the permeability of bi-directional textile fabrics. Compos Part A-Appl S 2006;37(5):679-694.

12. Endruweit A, McGregor, Long AC, Johnson MS. Influence of the fabric architecture on the variations in experimentally determined in-plane permeability values. Compos S Technol 2006;66(11-12):1778-1792.

13. Desplentere F, Lomov SV, Woerdeman DL, Verpoest I, Wevers M, Bogdanovich A. Micro-CT characterization of variability in 3D textile architecture. Compos Part A-Appl S 2005;36(6):1920-1930.

14. Desplentere F, Lomov SV, Verpoest I. Validation of stochastic mould filling simulations with correlated permeability fields. Proceedings of the 8th International Conference on Textile Composites, Nottingham, UK, 2006. p. T18/1-T18/6.

15. Markicevic B, Heder D, Advani SG, Walsh S. Stochastic modelling of preform heterogeneity to address dry spot formation in the VARTM process. Compos Part A-Appl S 2005;36(6):851-858.

16. Hoes K, Sol H, Dinescu D, Lomov SV, Parnas R Study of nesting induced scatter of permeability values in layered reinforcement fabrics. Compos Part A-Appl S 2004; 35(12): 1407-1418

17. Padmanabhan SK, Pitchumani R. Stochastic analysis of isothermal cure of resin systems. Polym Compos 1999;20(1):72-85.

18. Mawardi A, Pitchumani R. Cure cycle design for thermosetting matrix composites fabrication under uncertainty. Ann Oper Res 2004; 132(1-4):19-45.

19. Acquah C, Datskov I, Mawardi A, Zhang F. Achenie LEK, Pitchumani R, Santos E. Optimization under uncertainty of a composite fabrication process using a deterministic one-stage approach. Comput Chem Eng 2006; 30(6-7):947-960.

20. Li H, Foschi R, Vaziri R, Ferland G, Poursatip A. Probability-based modelling of composites manufacturing and its application to optimal process design. J Compos Mater 2002;36(16):1967-1991.

21. Escofet J, Millan MS, Rallo M. Modeling of woven fabric structures based on Fourier image analysis. Appl Optics 2001;40(34):6170-6176.

22. Millan MS, Escofet J. Fourier-domain-based angular correlation for quasiperiodic pattern recognition. Applications to web inspection. Appl Optics 1996;35(31):6253-6260.

23. Chan CH, Pang GKH. Fabric defect detection by Fourier analysis. IEEE Trans Industr Applic 2000;36(5):1267-1276.

24. Rallo M., Escofet J, Millan MS. Weave-repeat identification by structural analysis of fabric images. Appl Optics 2003;42(17):3361-3372.

25. Walsh JB. An introduction to stochastic partial differential equations. Lect Notes Math 1986;1180:265-439.

26. Terdik G, Woyczynski WA. Notes on fractional Ornstein-Uhlenbeck random sheets. Publ Math Debrecen 2005;66(1-2):53-181.

27. Arató M, Pap G, Van Zuijlen MCA. Asymptotic inference for spatial autoregression and orthogonality of Ornstein-Uhlenbeck sheets. Comput Math Appl 2001;42(1-2):219-229.

28. Ying Z. Maximum likelihood estimation of parameters under a spatial sampling scheme. Ann Stat 1993;21(3):1567-1590.

29. Ying Z. Asymptotic properties of a maximum likelihood estimator with data from a Gaussian process. J Multivariate Anal 1991;36(2):280-296

30. Fylstra D, Lasdon L, Watson J, Waren A. Design and use of the Microsoft Excel Solver. Interfaces 1998;28(5):29-55.

31. Skordos AA, Monroy Aceves C, Sutcliffe MPF. A simplified rate dependent model of forming and wrinkling of pre-impregnated woven composites. in press Compos Part A-Appl S.

32. Potluri P, Parlak I, Ramgulam R, Sagar TV. Analysis of tow deformations in textile preforms subjected to forming forces. Compos S Techol 2006;66(2):297-305.

33. Nguyen M, Herszberg I, Paton R. The shear properties of woven carbon fabric. Compos Struct 1999;47(1-4):767-779.

34. Kelly JM. Generalisation of some elastic-viscoplastic stress-strain relations. T Soc Rheol 1967;11(1):55-76

35. Sharma SB, Sutcliffe MPF, Chang SH. Characterisation of material properties for draping of dry woven composite material. Compos Part A -Appl S 2003;34(12):1167-1175.

36. Skordos AA, Monroy Aceves C, Sutcliffe MPF. Drape optimisation in woven composite manufacturing. Proceedings of the 5th International Conference on Inverse Problems in Engineering, vol. III. Cambridge, UK: Leeds University Press, 2005. p. S09.

Figure 1. Image analysis of carbon/epoxy pre-preg: (a) Image and identified unit cell positions; (b) FFT spectrum rotated by p/2; (c) Correlation distribution and identified unit cell positions.

Figure 2. Probability distributions of the unit cell variables 5 harness satin weave carbon/epoxy pre-preg: (a) Warp direction; (b) Weft direction; (c) Unit cell length in the warp direction; (d) Unit cell length in the weft direction.

Figure 3. Directional autocorrelation of tow orientation of the 5 harness satin weave carbon/epoxy pre-preg in (a) warp direction; and (b) weft direction. The legend reports the centre of bins. Each bin corresponds to a range of 25^{o}. Angles are measured in the clockwise direction with respect to the nominal warp direction.

Figure 4. Woven textile generation algorithm. (a) Generation of vertical boundary node. (b) Generation of horizontal boundary node. (c) Generation of internal node.

Figure 5. Simulation of the five harness satin weave carbon epoxy pre-preg using the Ornstein-Uhlenbeck model on a 10 mm spaced 20 × 20 grid. (a) Directional autocorrelation of weft orientation in the warp direction for two realisations of the stochastic model. (b) Realisation 1. (c) Realisation 2.

Fig. 6. Truss representation of a woven textile (a) Model assembly. (b) Unit cell.

Fig. 7. Comparison between experimental and model results in (a) tension and (b) bias extension of 5 harness satin weave carbon/epoxy pre-preg.

Fig. 8. Forming simulation of the five harness satin weave carbon epoxy pre-preg. Comparison of (a) shear angle and (b) engineering wrinkling strain distributions using constant peripheral holding force; with model (c) shear angle (d) engineering wrinkling strain distributions using variable peripheral holding force. The total blank holder force is 400 N in both cases. In the variable force profile nodal force at diagonal positions is increased by 75%.

Fig. 9. Stochastic simulation of the forming of the five harness satin weave carbon epoxy pre-preg. Comparison of probability distributions of (a) average wrinkling strain and (b) minimum wrinkling strain, under uniform and variable peripheral holding force profiles. The dashed lines indicate the strain in the

case of forming of an ideal textile. The total blank holder force is 400 N in both cases and the number of realisations is 400.

Fig. 10. Stochastic simulation of the forming of the five harness satin weave carbon epoxy pre-preg: (a) Woven textile realisat ion. (b) Wrinkling strain distribution for uniform peripheral holding force. (c) Wrinkling strain distribution for variable peripheral force. The total blank holder force is 400 N in both cases. In the variable force profile nodal force at diagonal positions is increased by 75%.

Table 1

Statistical properties of unit cell parameters of 6k carbon/1947 epoxy 5 harness satin weave

Variable	μ	s	s_r	s_u
$?_{warp}\left(^{o}\right)$	-0.10	0.36	0.16	0.10
$?_{weft}\left(^{o}\right)$	89.68	0.95	0.10	0.10
$l_{warp}/l_o\,(\%)$	99.81	1.10	2.00	0.18
$l_{weft}/l_o\,(\%)$	99.10	0.81	1.32	0.18

Table 2

Correlation matrix of unit cell parameters of 6k carbon/1947 epoxy 5 harness satin weave

Variable	$?_{warp}$	$?_{weft}$	l_{warp}/l_o	l_{weft}/l_o
$?_{warp}$	1.00	0.03	0.13	0.00
$?_{weft}$	0.03	1.00	0.09	0.00
l_{warp}/l_o	0.13	0.09	1.00	-0.06
l_{weft}/l_o	0.00	0.00	-0.06	1.00

Table 3

Material model parameters for the five harness satin weave epoxy pre-preg

$s_o(N/tow)$	$?_o(Ns/tow)$	s_o	s_∞	a_v	$\bar{e}_v$	$E_v(N/tow)$	$E_p(N/tow)$	$E_o(N/tow)$	$E_\infty(N/tow)$	$\bar{e}$	a
0.0334	3.622	24.64	3995.2	17.05	0.458	9.970	0.861	11261	49846	0.0014	5990.9

Table 4

Average and minimum engineering wrinkling strain and maximum shear angle predicted by the simulation of hemisphere forming of the five harness satin weave carbon epoxy pre-preg

	Average wrinkling	Minimum wrinkling	Maximum shear (^{o})
Constant force	$-0.244\ 10^{-2}$	-0.107	53.88
Variable force	$-0.142\ 10^{-2}$	-0.078	54.46

Table 5

Statistical properties of average and minimum engineering wrinkling strain predicted by stochastic forming simulation

		Average wrinkling (%)		Minimum wrinkling	
		μ	s	μ	s
Constant force	Warp tows	-0.244	0.031	-0.131	0.015
	Weft tows	-0.245	0.032	-0.134	0.019
	Total	-0.245	0.017	-0.142	0.017
Variable force	Warp tows	-0.159	0.024	-0.105	0.016
	Weft tows	-0.160	0.023	-0.110	0.020
	Total	-0.159	0.013	-0.118	0.017

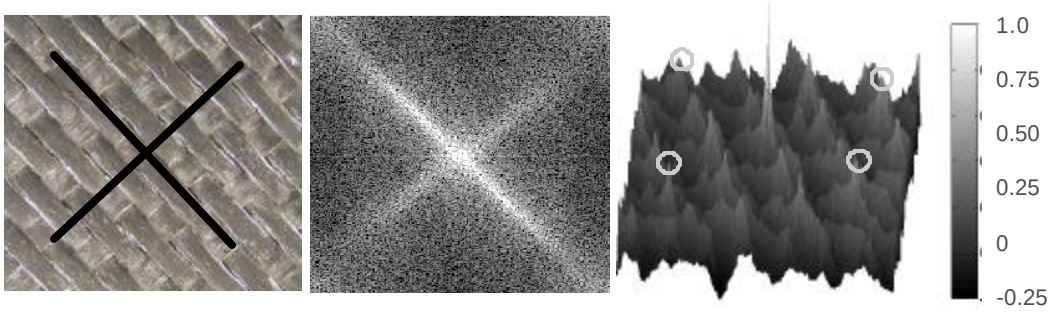

(a) (b) (c)

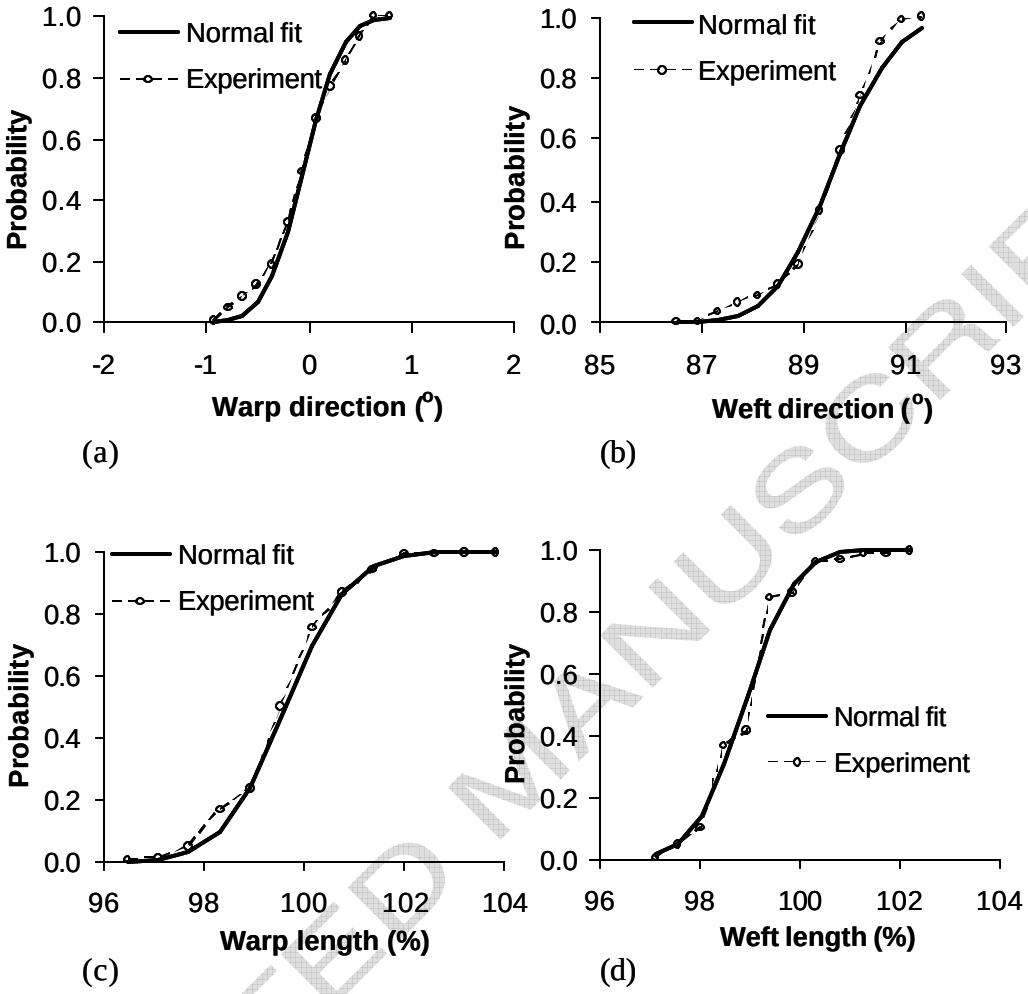

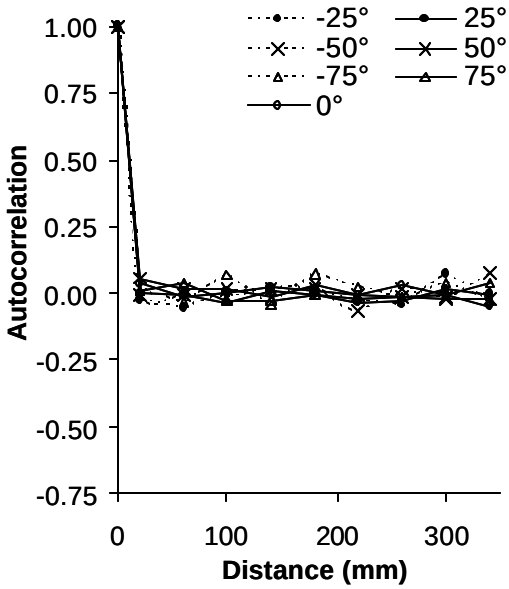

(a)

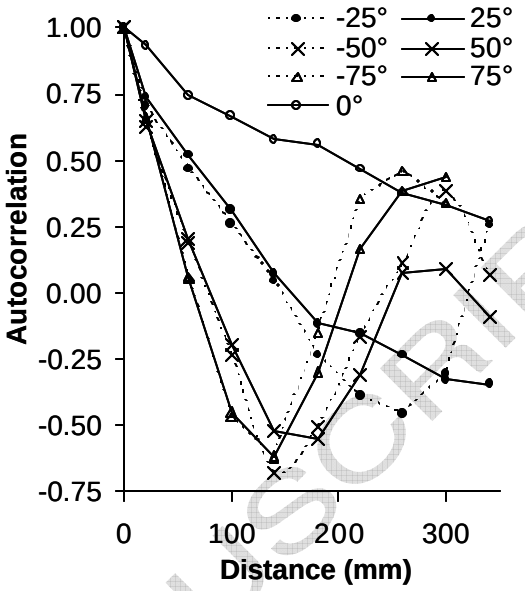

(b)

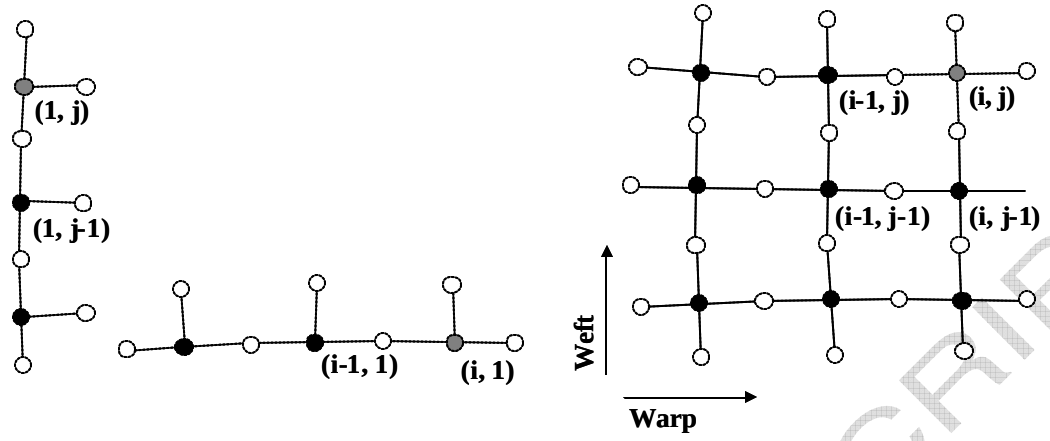

(a) (b) (c)

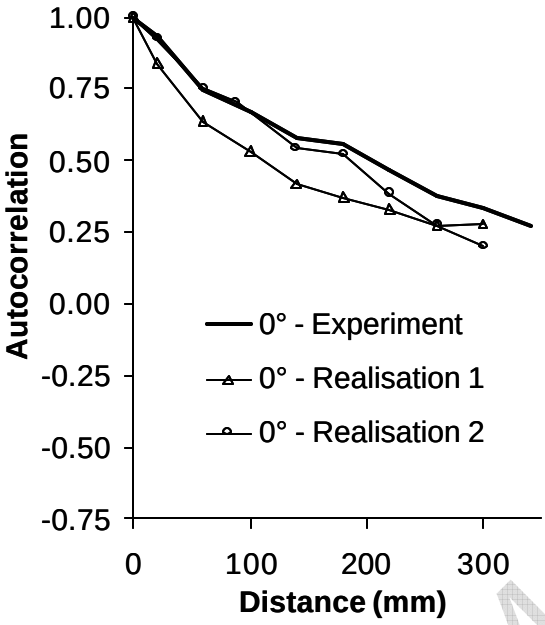

(a)

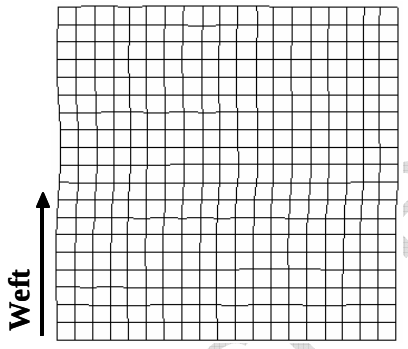

(b)

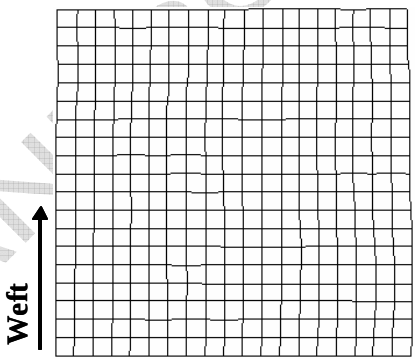

(c)

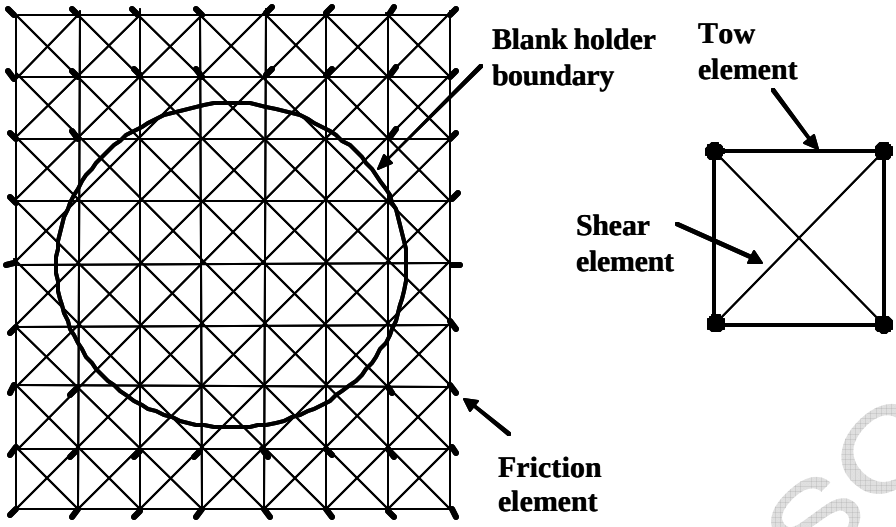

(a) (b)

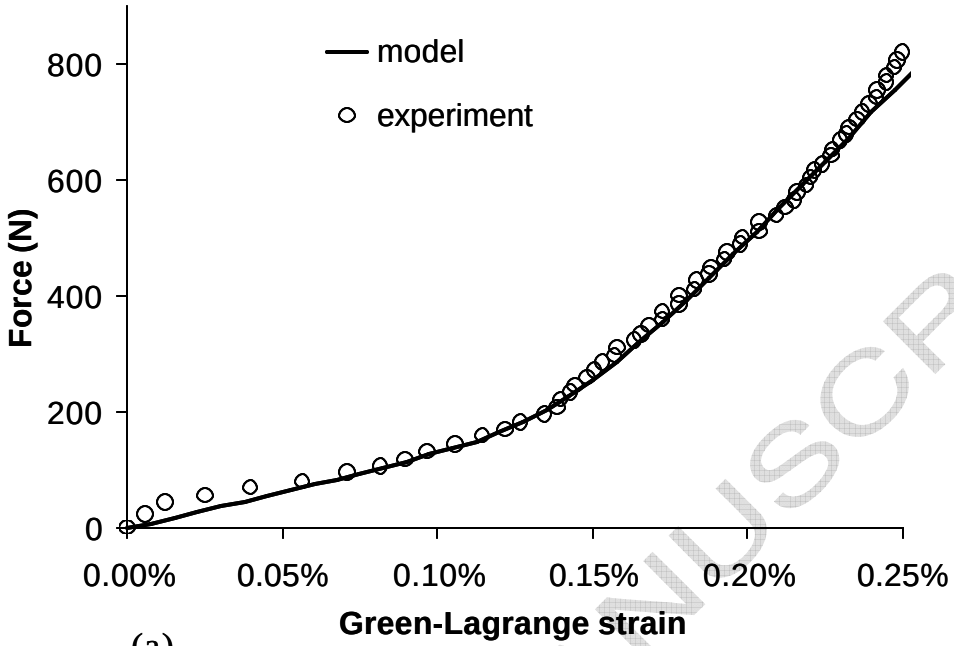

(a)

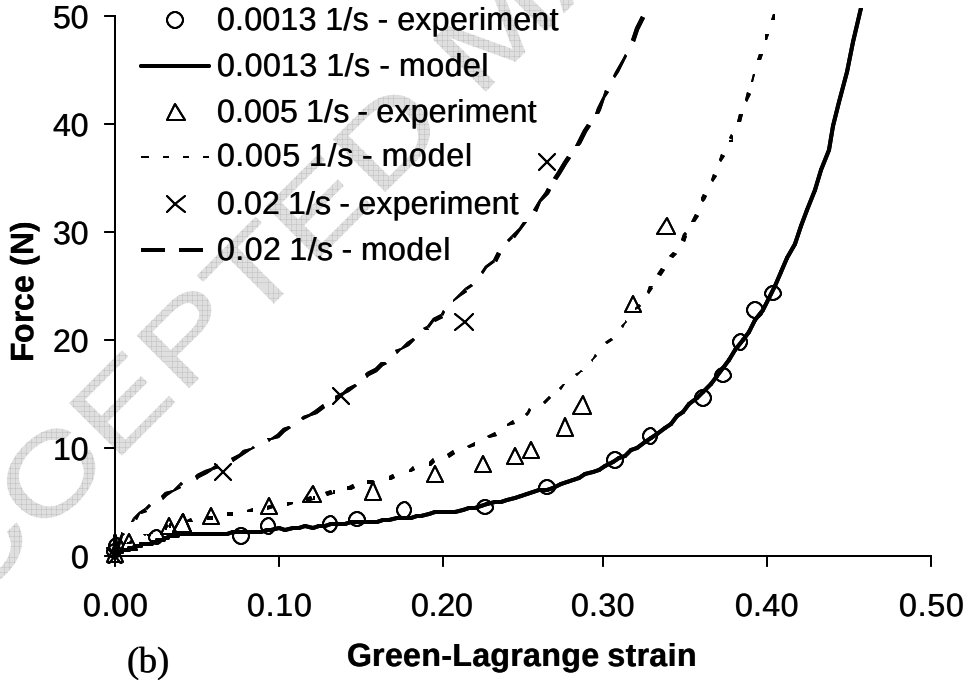

(b)

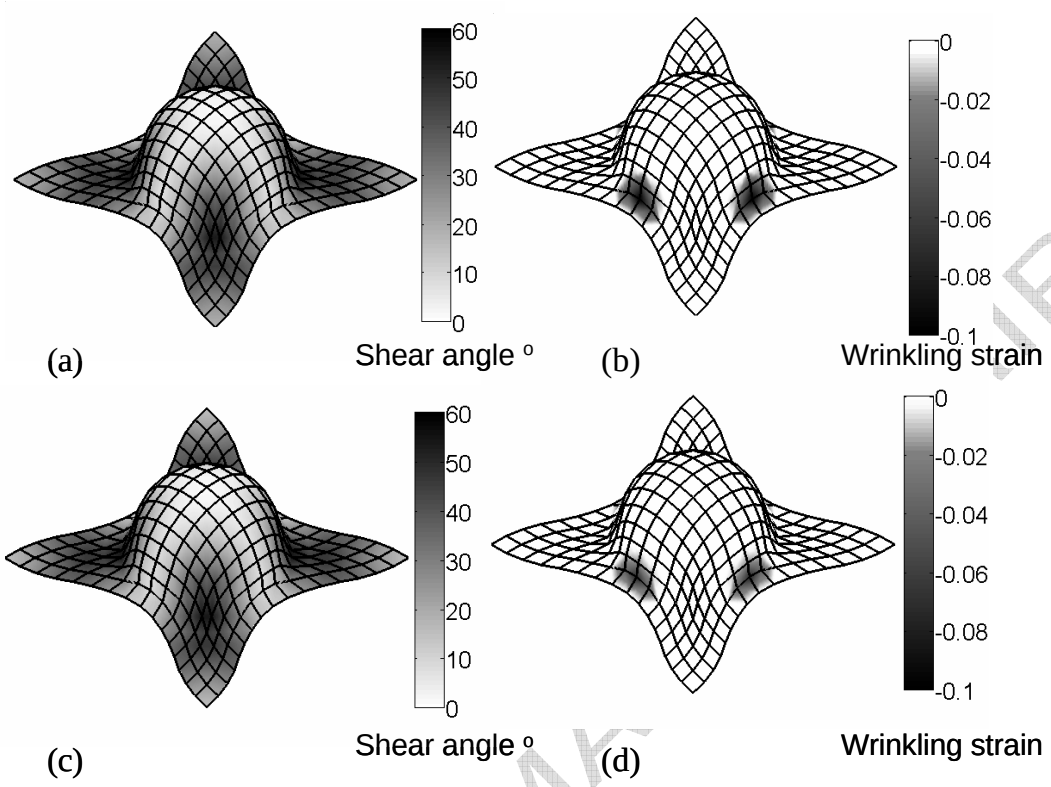

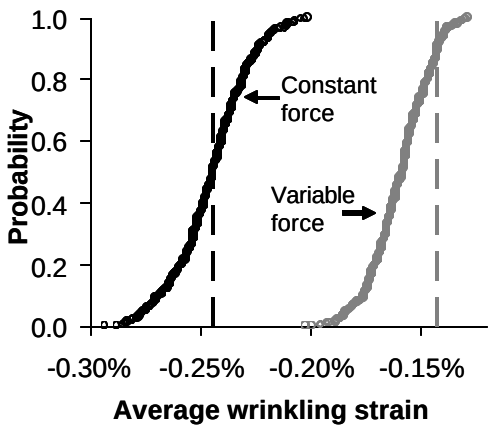

(a)

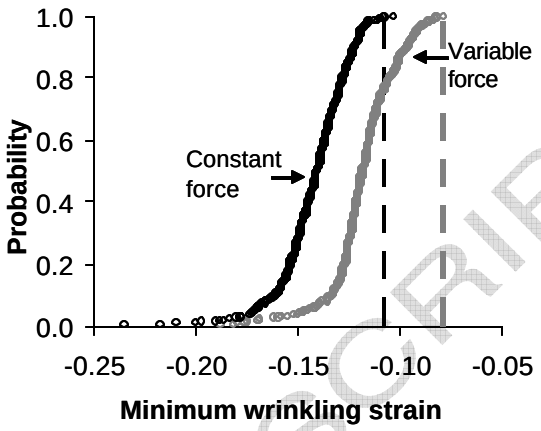

(b)

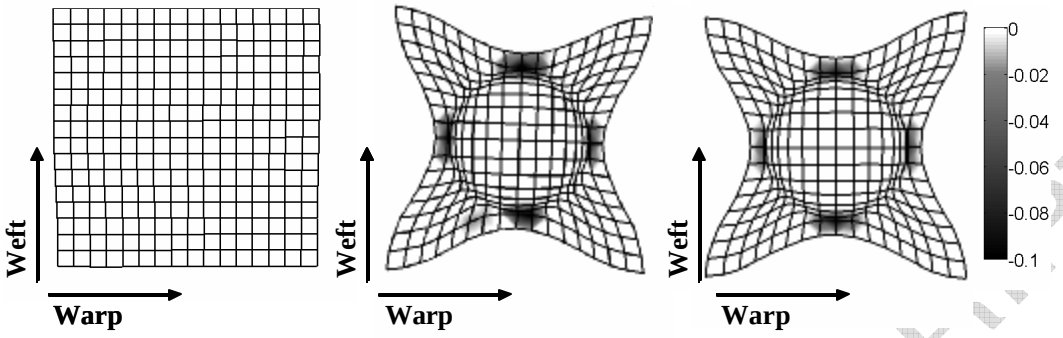

(a) (b) (c)